Organic Geochemistry 195 (2024) 104847

Contents lists available at ScienceDirect

Organic Geochemistry

journal homepage: www.elsevier.com/locate/orggeochem

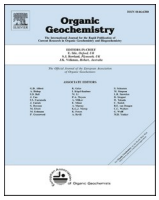

Soil chemistry effect on GDGT abundances and their proxies in soils of the Okavango Delta

Julie Lattaud [a,1,*], Mangaliso J. Gondwe [b], Marco Griepentrog [c], Carole Helfter [d], Cindy De Jonge [a]

[a] Biogeoscience Group, Geological Institute, ETH Zurich, Zurich, Switzerland
[b] Okavango Research Institute (ORI), University of Botswana, Maun, Botswana
[c] Soil Resources, Department of Environmental Systems Science, ETH Zurich, Zurich, Switzerland
[d] UK Centre for Ecology and Hydrology, Penicuik EH26 0QB, UK

ARTICLE INFO

Associate editor: John Volkman

Keywords:
Botswana
Paleoenvironment
brGDGTs
isoGDGTs
MBT'_{5ME}
TEX_{86}
Ri/b
Wetlands

ABSTRACT

Branched and isoprenoid glycerol dialkyl glycerol tetraethers (brGDGTs, and isoGDGTs) are two families of membrane lipids commonly used to reconstruct paleo-environmental parameters. Their use as a quantitative proxy for past temperatures has been hindered by the discovery of other environmental controls on their distribution in soils, such as changes in bacterial community composition, chemistry and aridity. To test for the impact of aridity-driven soil chemistry changes, GDGT concentrations and derived proxies were measured in 43 soils along a chemical gradient in the Okavango Delta. All brGDGT concentrations increase with decreasing pH. Alkalinity-promoted (6-methyl and cyclopentane-containing) brGDGTs show a secondary concentration increase in arid soils, characterized by a high pH>8 and cation exchange capacity (CEC>30 cmolc kg^{-1}). The concentration of 5-methyl brGDGTs increases faster that of 6-methyl brGDGTs in arid compared with non-arid soils. Although limited variability in temperature is present (~2 °C), significant variation in MBT'_{5ME} values is observed (0.63–0.96) likely driven by the variation in CEC. IsoGDGTs are present in lower concentrations than brGDGTs, and Ri/b values, a potential proxy for paleohydrological reconstruction, correlating with soil water content ($r = 0.45$, $p < 0.01$). TEX_{86} values (0.57–0.97) correlate with pH across the aridity transect. In this region, where accurate proxies and quantitative paleostudies are scarce, the impact of aridity-driven chemistry changes on GDGT-proxies is shown, i.e., MBT'_{5ME} is overall controlled by CEC, but correlates negatively with pH in non-arid soils and with IR_{6ME} in arid alkaline soils. Furthermore, we propose GDGT-based proxies for concentration in exchangeable calcium, past hydrological changes and soil pH.

1. Introduction

Understanding how temperature varied in the past in response to climate and environmental changes is essential to refine climate models and better forecast Earth's future. There is a wide range of lipid biomarkers, i.e., lipid molecules that contain information on the environmental conditions of the biological producer. An example of a well-studied lipid biomarker group is the glycerol dialkyl glycerol tetraethers (GDGTs), which are widely present in marine and freshwater water columns and sediments, as well as soils (e.g., Schouten et al., 2013). Two types of GDGTs exist: isoprenoid (iso) and branched (br) GDGTs. Branched GDGTs (Supplementary Fig. S1 shows chemical structures), are commonly used in the terrestrial realm to reconstruct paleoenvironmental parameters such as temperature or pH. The compounds can be tetra- (brGDGT-I), penta- (brGDGT-II) or hexamethylated (brGDGT-III), with the location of the additional outer methyl branches on the α-5 (5-methyl) or α-6 (6-methyl) position (De Jonge et al., 2014a). Furthermore, brGDGTs can have different numbers of internal cyclizations (0–2, respective structures annotated with a, b, and c, respectively). Based on correlations between brGDGTs and bacterial DNA counts in soils the phylum Acidobacteria contains probable brGDGT producers (Weijers et al., 2009), although not all acidobacterial cultures can produce brGDGTs (e.g., Sinninghe Damsté et al., 2011; 2018). While 5-methyl brGDGTs have been recently found in to be produced by the

* Corresponding author.
E-mail address: Julie.lattaud@unibas.ch (J. Lattaud).
[1] Now at Department of Environmental Sciences, University of Basel, Basel, Switzerland.

https://doi.org/10.1016/j.orggeochem.2024.104847
Received 20 March 2024; Received in revised form 29 July 2024; Accepted 29 July 2024
Available online 31 July 2024

cultured acidobacterial strain *Solibacter usitatus* (Halamka et al., 2021, 2023; Chen et al., 2022), 6-methyl isomers have not been found in culture yet. A restricted bacterial source is surmised, as Halffman et al. (2022) found a link between an increase in contribution of Acidobacteria subgroup 6, the production of 6-methyl brGDGTs, and the concentration of exchangeable calcium.

The relative abundance of tetramethylated brGDGTs (Ia, Ib, Ic) and brGDGT-IIa and IIIa varies with temperature, both in the environment along gradients in temperature and in cultures exposed to different growth conditions (e.g., De Jonge et al., 2014a; Chen et al., 2022; Halamka et al., 2023). In addition to temperature, a variety of other environmental parameters, e.g. vegetation (Davtian et al., 2016, Liang et al., 2019), bacterial community composition (De Jonge et al., 2019; Halffman et al., 2022), the soil water content (Loomis et al., 2011; Menges et al., 2014; Dang et al., 2016a; Dang et al., 2016b; Duan et al., 2022; Guo et al., 2022), oxygen level (Pei et al., 2021), pH (e.g., Duan et al., 2020; Chen et al., 2021; Guo et al., 2022; Häggi et al., 2023) and soil chemistry (De Jonge et al., 2021, 2024; Véquaud et al., 2021; Halffman et al., 2022) have been shown to impact the distribution of brGDGTs in soils and potentially bias the application of brGDGT-based paleoclimate proxies. In this respect, arid and non-arid soils have shown striking differences in term of brGDGT-proxy relation to environmental parameters (e.g., Xie et al., 2012; Yang et al., 2014; Dugerdil et al., 2021; Guo et al., 2021; 2022; Wang et al., 2024). In arid soils in Mongolia, CBT' has been shown to correlate with pH in low pH (<7) soils but not in the arid ones where it correlates with soil moisture content (Wang et al., 2014). Similarly, at pH<3.5, MBT'$_{5ME}$ correlated with free acidity (De Jonge et al., 2021). In these studies, soil moisture usually refers to aridity caused by climate (precipitation below 500 mm y^{-1}) or altitudinal differences and not the moisture present intrinsically in the soils. Arid and non-arid soils have a fundamentally different soil chemistry (Zhang and Wienhold, 2002; Slessarev et al., 2016). As changes in soil chemistry can have a large impact on environmental brGDGT distribution (De Jonge et al., 2019, 2021, 2024; Guo et al., 2022; Halffman et al., 2022), the proposed impact of soil moisture and aridity can be targeted by taking a diverse suite of soil chemical parameters into account.

IsoGDGTs are membrane-spanning lipids produced by a wide range of archaea (e.g., Schouten et al., 2013). They can have a different number of cyclopentane rings (ranging from 0 to 8 rings) and can contain a cyclohexane ring in the case of the compound crenarchaeol (Sinninghe Damsté et al., 2002). Crenarchaeol is a biomarker specific for Thaumarchaeota, while isoGDGT-0 can be produced by a large range of archaea (e.g., Schouten et al., 2013). As different Thaumarchaeotal groups produce isoGDGT-0 to -3, crenarchaeol and crenarchaeol isomer in different proportions (e.g., Schouten et al., 2013), the distribution of isoGDGTs can be used as a taxonomic fingerprint. As Thaumarchaeota group 1.Ib is more present in dry alkaline and aerated soils (Auguet et al., 2010; Bates et al., 2011), whereas groups 1.Ia, 1.Ia-associated and I.1c prefer acidic soils (Tripathi et al., 2013; Weber et al., 2015), specific isoGDGT ratios (Fcren'; Baxter et al., 2021) are expected to vary across large pH gradients in soils. Aside from Thaumarchaeota, *Bathyarchaeota* and *Methanobacteria* also produce isoGDGTs (dominantly isoGDGT-0, Zheng et al., 2019). These archaea are more abundant in moist soils (Vaksmaa et al., 2016), and the isoGDGT-0/cren ratio will thus vary across soil moisture gradients. When Thaumarchaeota are the dominant producers, TEX$_{86}$, the ratio of isoGDGT-2, isoGDGT-3 and crenarchaeol isomer against isoGDGT-1 can be used to reconstruct air temperature in soils (Schouten et al., 2002; Coffinet et al., 2014; Yang et al., 2016). However, most studies report only a weak correlation with temperature which is explained by the effect of shifts in the composition of the isoGDGT-producing archaeal community (e.g., Xie et al., 2015; Li et al., 2018; Zheng et al., 2019; De Jonge et al., 2024). As archaeal isoGDGT lipids become relatively more abundant, compared with bacterial brGDGTs in arid soils, the BIT index and Ri/b indices correlate with soil moisture in arid and non-arid soils (e.g., Xie et al., 2012; Dirghangi et al., 2013; Wang et al., 2014; Dang et al., 2016a; Dang et al., 2016b). To study the impact of changes in aridity-driven soil chemistry along a soil transect in semi-arid south Africa, we studied 43 soil samples in the Okavango Delta, covering seasonal and annual variation in aridity and associated soil chemistry changes (2018–2020). These soils experience the same temperature (variation within the transect is less than 2 °C) and have a similar vegetation cover, but they include examples of arid and non-arid soils, where the non-arid soils experience varying degrees of seasonal inundation. The relationships between brGDGTs, isoGDGTs and selected soil chemistry parameters (exchangeable cations, pH, water content, conductivity) were investigated to assess their effect on GDGT-derived proxies. Specifically, the study aims to deconvolute the effect of soil chemistry changes associated with arid and non-arid soils on brGDGT proxies MBT'$_{5ME}$ and CBT', and isoGDGT distributions in the context of future regional paleo-reconstructions.

2. Material and methods

2.1. Study sites

Chiefs Island is one of the Okavango Delta's permanent islands, located in a seasonal swamp area with a semi-arid center (Fig. 1). Flooding in the Delta typically peaks in August, nearly four months after the summer rain in Angola (Ellery et al., 1993; Gumbricht et al., 2004a, 2004b). During the austral winter months (June to September), the water level in the Boro channel (nearby Chiefs Island) is at its peak. This is followed by the warm rainy season that lasts from November to March (averaging 490 mm yr^{-1}, Gumbricht et al., 2004a; Gondwe et al., 2021).

43 soil samples were collected were collected in the Okavango Delta between 2018 and 2021 as part of the NERC funded MOYA "Closing the global methane budget" project, implemented by the UK Centre for Ecology and Hydrology (UKCEH) and the Okavango Research Institute of the University of Botswana (Fig. 1). The sampling sites are defined by their respective distance from site 1 whose location was fixed throughout the sampling period (Table 1). As the transect was partly located in the floodplain, and only non-submerged soils were sampled, the transect varied in length. As such, it had a maximum length of 260 m and 7 sites during the low-flood season (February, March), while during the high-flood season (August, September) the transect only had 5 sites (~55 m). C_4 grasses (*Imperata cylindrica*, *Eragrostis inamoena*, *Miscanthus junceus*) were dominant around site 1 to 3 across the seasons, whereas for site 4 to 7 (seasonally flooded sites), C_4 plants were dominant during the low-flood season while macrophytes (C_3 plants) were present during the high-flood season. These soils are arenosols which consist predominantly of sands (up to 85%) with an increase in peat and other organic material closer to the river (site 4 to 7), thus creating an 'O' horizon in the lower seasonal floodplains (Gondwe et al., 2021).

In summary, the soil samples were taken in triplicate at 0–10 cm depth, oven-dried (at 105 °C), with electrical conductivity, soil temperature, pH, soil organic carbon (TOC) and soil water content previously reported in Gondwe et al. (2021). Soil water content (in %) was defined as the ratio of the mass of water present to the dry weight of the soil sample (Gondwe et al., 2021).

2.2. Lipid extraction and quantification

Freeze-dried soils (2–3 g) were ground and extracted with an EDGE system (CEM) as described in Lattaud et al. (2021). Following extraction, the total lipid extract was saponified with 0.5 M potassium hydroxide (KOH) in methanol (MeOH) to remove the fatty acids, and the neutral fraction was liquid–liquid extracted three times with hexane. The remaining saponified products were acidified (pH ~2) and the neutral fraction was liquid–liquid extracted with Hex:DCM (4:1, v/v) three times. The neutral fraction was further separated over a silica gel column (deactivated 1%) into two fractions with Hex:DCM (9:1, v/v), and DCM:MeOH (1:1, v/v). The second fraction contains the GDGTs. An

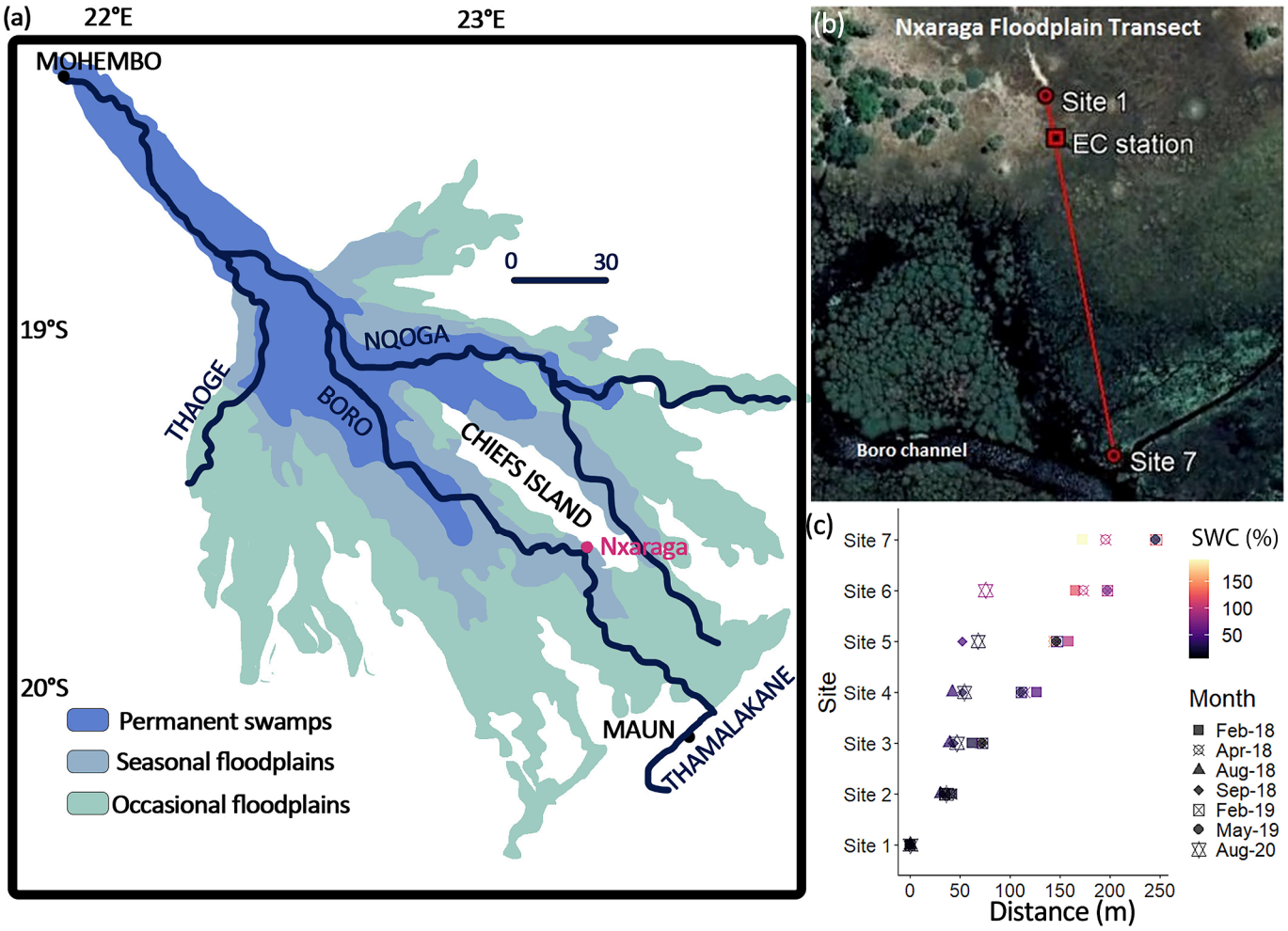

Fig. 1. (a) Sampling location at the Nxaraga transect, Okavango Delta (Botswana), scale bar indicates 0–30 km, and (b) aerial photo of the transect, adapted from Gondwe et al. (2021), (c) sampling sites and their distance from site 1. Symbols are colored according to their soil water content (SWC in %).

internal standard (C_{46} GDGT, Huguet et al., 2006) was added to the GDGT fraction which was subsequently filtered on a polytetrafluoroethylene filter (0.45 μm pore-size).

Branched and isoGDGTs were analysed with high performance liquid chromatography (LC)/atmospheric pressure chemical ionization–mass spectrometry (MS) on an Agilent 1260 Infinity series LC-MS (Hopmans et al., 2016) using two Waters Acquity UHPLC BEH hydrophilic liquid interaction chromatography (HILIC) columns (1.7 μm; 2.1 × 150 mm). The columns were heated to 45 °C and the flow rate was set to 0.2 mL min^{-1}. The UHPLC was coupled to an Agilent 6130 single quadrupole mass spectrometer. Selective ion monitoring of the $[M+H]^+$ was used to detect and quantify the different GDGTs (Huguet et al., 2006), and a similar response factor was assumed for the GDGTs and the internal standard. Concentrations are based on the peak areas of each GDGT's specific ion and the internal standard, normalized per g of soil extracted. Based on a long-term laboratory standard the analytical uncertainty is 0.02 for MBT'_{5ME} and 0.03 for IR values. Several ratios were calculated and calibrated to calculate pH (De Jonge et al., 2014b, 2021):

$$MBT'_{5ME} = \frac{(Ia + Ib + Ic)}{(Ia + Ib + Ic + IIa + IIb + IIc + IIIa)} \quad (1)$$

$$CBT' = \log10[\frac{(Ic + IIa' + IIb' + IIIa' + IIIb' + IIIc')}{(Ia + IIa + IIIa)}] \quad (2)$$

$$IR_{6ME} = \frac{IIa' + IIIa' + IIb' + IIc'}{IIa + IIa' + IIb + IIb' + IIc + IIc' + IIIa + IIIa'} \quad (3)$$

$$pH = 7.15 + 1.59 \times CBT' \quad (4)$$

As soil chemistry is the main target of this paper, we tested the proposed ratio to reconstruct exchangeable Ca^{2+} ([Eq 11] from De Jonge et al., 2024).

$$\frac{Ib + IIa' + IIb'}{\sum \text{all brGDGT}} \quad (5)$$

For isoGDGTs, the TEX_{86} was calculated as follows (Schouten et al., 2002):

$$TEX_{86} = \frac{GDGT-2 + GDGT-3 + \text{cren isomer}}{GDGT-1 + GDGT-2 + GDGT-3 + \text{cren isomer}} \quad (6)$$

The ratio of isoGDGT and brGDGT from Xie et al. (2012) was calculated (i.e., Ri/b).

$$Ri/b = \frac{\sum \text{isoGDGT}}{\sum \text{brGDGT}} \quad (7)$$

2.3. Exchangeable cation measurements

2.5 g of freeze-dried milled soils (each being a combination of three sample replicates) were shaken for 2 h with 25 mL of ammonium acetate (NH_4Ac, 1 M, pH=7.0) to extract the cations. After settling, the pH was measured with a 713 pH meter (Metrohm). This pH was used to calculate back the amount of free hydrogen ions (H^+) based on a NH_4Ac

Table 1
Soil sampling locations and date sampled, as well as their distance from site 1, soil water content* (SWC in %), and soil temperature* (°C) (Gondwe et al., 2021).

Date sampled	Site #	Latitude (°S)	Longitude (°E)	Distance from site 1 (m)	SWC (%)	Soil temp at the time of sampling (°C)
Feb-18	1	19.547883	23.179050	0.00	8.840	31.13
Feb-18	2	19.548250	23.179117	42.4	17.304	29.03
Feb-18	3	19.548417	23.179217	62.5	24.449	29.47
Feb-18	4	19.549000	23.179400	127.0	50.993	27.37
Feb-18	5	19.549267	23.179300	158.6	94.611	27.30
Feb-18	6	19.549383	23.179200	165.4	120.993	27.10
Feb-18	7	19.549400	23.179083	172.4	190.285	25.67
Apr-18	1	19.547883	23.179033	0.0	9.660	27.67
Apr-18	2	19.548233	23.179150	40.7	8.550	24.30
Apr-18	3	19.548483	23.179267	71.0	54.670	24.97
Apr-18	4	19.548867	23.179350	114.2	62.581	25.27
Apr-18	5	19.549133	23.179400	144.2	139.830	26.83
Apr-18	6	19.549383	23.179483	173.3	97.181	25.13
Apr-18	7	19.549600	23.179467	196.2	97.194	26.33
Aug-18	1	19.547910	23.179060	0.0	17.249	18.43
Aug-18	2	19.548180	23.179100	30.3	25.070	17.73
Aug-18	3	19.548250	23.179160	39.2	35.859	18.13
Aug-18	4	19.548290	23.179070	42.2	39.159	19.40
Aug-18	5	19.548410	23.179110	55.8	53.751	22.70
Sep-18	1	19.547930	23.179080	0.0	20.562	19.33
Sep-18	2	19.548220	23.179070	32.2	34.645	18.60
Sep-18	3	19.548320	23.179070	43.3	26.150	20.00
Sep-18	4	19.548400	23.179080	52.2	28.271	22.33
Sep-18	5	19.548400	23.179090	52.2	47.209	23.17
Feb-19	1	19.547910	23.179100	0.0	12.026	27.98
Feb-19	2	19.548250	23.179140	34.5	7.234	28.67
Feb-19	3	19.548580	23.179280	72.6	21.244	28.63
Feb-19	4	19.549000	23.179350	111.1	41.899	28.28
Feb-19	5	19.549420	23.179470	147.0	44.433	28.50
Feb-19	6	19.549690	23.179600	197.5	90.589	28.22
Feb-19	7	19.549900	23.179540	246.4	121.379	28.93
May-19	1	19.547930	23.179130	0.0	6.716	25.60
May-19	2	19.548240	23.179150	34.5	4.310	25.20
May-19	3	19.548580	23.179200	72.6	5.018	27.17
May-19	4	19.548910	23.179340	111.1	28.110	26.10
May-19	5	19.549220	23.179440	147.0	9.771	25.50
May-19	6	19.549660	23.179560	197.5	69.351	26.37
May-19	7	19.550080	23.179700	246.4	24.389	26.17
Aug-20	1	19.547917	23.179111	0.0	12.767	18.20
Aug-20	2	19.548222	23.179167	36.1	14.664	18.27
Aug-20	3	19.548333	23.179167	46.6	22.550	17.00
Aug-20	4	19.548417	23.179194	54.2	23.078	17.53
Aug-20	5	19.548528	23.179222	68.0	20.959	17.67
Aug-20	6	19.548583	23.179250	75.4	83.156	20.00

*FromGondwe et al., 2021.

titration curve (Brown, 1943). If the pH measured was > 7, no H^+ ions were available and free acidity was not calculated. Hence, free acidity is not calculated for the very alkaline soils (as the NH_4A-pH was above 7), and free acidity in these alkaline soils is assumed to be 0. The supernatant was filtered over a 0.45 μm filter and the filtered-extract was analysed for sodium (Na^+), calcium (Ca^{2+}), potassium (K^+), magnesium (Mg^{2+}), aluminum (Al^{3+}), iron (Fe^{3+}) and manganese (Mn^{2+}) cations by inductively coupled plasma – optical emission spectrometry (ICP-OES, 5100 ICP-OES, Agilent Technologies). The cation exchange capacity (CEC) is calculated as 2 × [Ca] + 2 × [Mg] + [Na] + [K] + 3 × [Al] + [H^+] (all in cmolc × kg soil^{-1}), the sum of all metals is 2 × [Mn] + 3 × [Fe] + 3 × [Al] and the sum of bases [Na] + [K] + 2 × [Ca] + 2 × [Mg].

2.4. Statistics and global calibration

All statistical analyses were performed using Rstudio (version 4.2.1, R Core Team, 2023), using the *FactoMineR* (Lê et al., 2008) and *corrplot* (Wei and Simko, 2021) packages. All correlations are considered significant if $p < 0.01$. Plots were realized using *ggplot2* (version 3.3.5; Wickham, 2009) and *factoextra* (Kassambara and Mundt, 2023).

MBT'_{5ME} and CBT′ were compared to a global dataset (Hopmans et al., 2016). The data compilation encompassed datasets from Weijers et al. (2007); De Jonge et al. (2014a); Dang et al. (2016a, 2016b); Ding et al. (2016); Wang et al. (2016); Xiao et al. (2016); Naafs et al. (2017); Jaeschke et al. (2018); Dearing Crampton-Flood et al. (2020); Dugerdil et al. (2021); Pérez-Angel et al. (2020); Duan et al. (2020, 2022); Chen et al. (2021); Guo et al. (2022); Peaple et al. (2022).

3. Results

3.1. Soil properties

Data from Gondwe et al. (2021) used as background information for this study include measured soil temperature, pH (Fig. 2a), soil water content (SWC, Fig. 1c), and total carbon content (TOC, Fig. 2d). SWC and TOC decrease with distance from the river channel ($r = 0.69$, $r = 0.53$, and $r = 0.41$, $p < 0.01$, respectively). pH values (4.7–10.5) increase with distance from the river channel ($r = 0.69$, $p < 0.01$), from acidic to alkaline values (Fig. 2a). Summarizing the dependency between chemical parameters, SWC is negatively correlated with pH ($r = –0.67$, $p < 0.01$), and positively with exchangeable Ca^{2+}, free acidity, metal cations and TOC ($0.65 < r < 0.79$, $p < 0.01$, Fig. 2g). TOC correlates strongly with CEC and the main cations ($r > 0.8$, $p < 0.01$). Exchangeable Ca^{2+} is the most abundant cation in the soils, with concentration up to 20 cmolc kg^{-1}, and as low as 1.9 cmolc kg^{-1} (Fig. 2b). Highest Ca^{2+} concentrations are encountered both close to the river bed

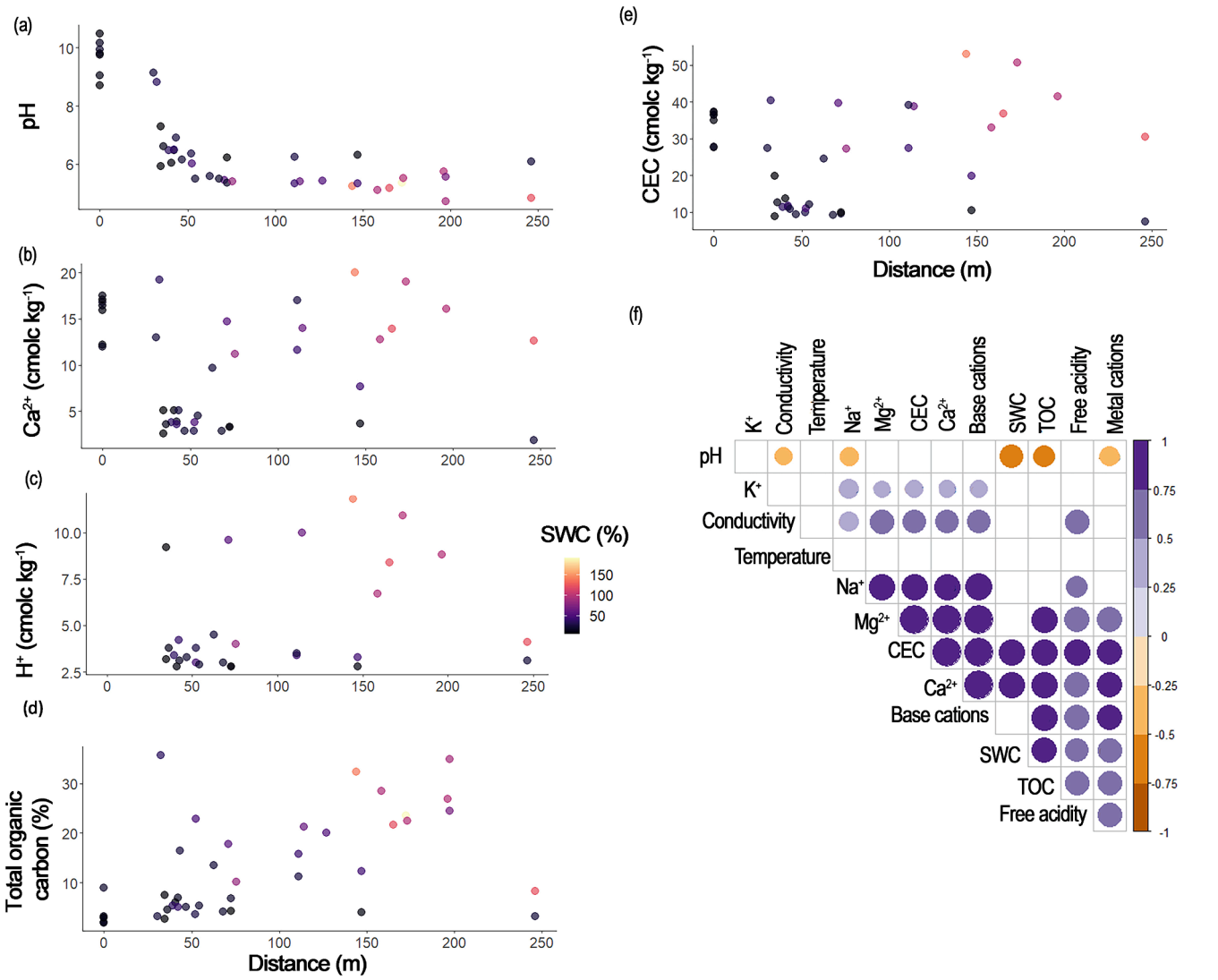

Fig. 2. Selected soil chemistry parameter values along the sampling transect (distance from Site 1 in m), (a) pH, (b) exchangeable Ca^{2+}, (c) free acidity (H^{+}), (d) cation exchange capacity (CEC), (e) soil carbon content (%) and (f) correlation matrix of the main soil chemistry parameters. Coefficients are provided in Supplementary Table S6.

and further away from it. Exchangeable Mg^{2+}, K^{+} and Na^{+} are also abundant in the soils but at a tenfold lower concentration (on average 1.5 ± 0.7, 0.7 ± 0.6 and 0.5 ± 0.5 cmolc kg^{-1}, respectively, Table 2). The concentrations of exchangeable Fe^{3+}, Al^{3+} and Mn^{2+} are very low and the sum of these metal cations is always below 0.2 cmolc kg^{-1} (Table 2), increasing with increasing SWC ($r = 0.72$, $p < 0.01$, Fig. 2f). The sum of base cations varies between 5.3 and 46.5 cmolc kg^{-1} and is independent from SWC, but correlates positively with TOC ($r = 0.8$, $p < 0.01$, Fig. 2f). Free acidity was highest at intermediate distance from the river channel (10.0 to 11.8 cmolc kg^{-1}, Fig. 2c). Soils with the highest CEC (7.7 ± 2.9 cmolc kg^{-1}) are found at intermediate distance (>150 m from site 1, Fig. 2d). CEC in the soils is driven by exchangeable Ca^{2+}, Mg^{2+}, free acidity and Na^{+} ($r = 0.99$, $r = 0.97$, $r = 0.83$, and $r = 0.81$, $p < 0.01$, respectively, Fig. 2f).

In summary there are three types of soils. Firstly, the arid soils that remain dry and are very alkaline with low TOC content, high electrical conductivity, high CEC. Secondly, the seasonally inundated soils closer to the river, characterized by lower pH, generally high CEC, medium to low electrical conductivity and higher TOC, metal cations concentration and soil water content. In these two types of soils Mg^{2+} and Ca^{2+} can be abundant and CEC values can be increased. The third type of soils is located in the middle of the transects and is neither semi-arid nor often inundated, and has low CEC values as well as neutral pH. There is no correlation between soil temperature at the time of sampling and any of the chemical soil parameters under study (Fig. 2f). To avoid the influence of seasonality, which is inherent to directly using the in-situ measured soil temperature at time of sampling, mean annual soil temperature (MAST) is calculated in three spatial ranges. Here, a first range captures the arid soils (0 m, n = 18, MAST=23.8 ± 9.0 °C±std.), a second range captures the non-arid soils (1 to 100 m from site 1, n = 26, MAST=22.3 ± 8.1 °C) and a third range captures the seasonally inundated sites (>100 m, n = 50, MAST=25.5 ± 5.3 °C), where the standard error mainly reflects seasonal variability.

3.2. BrGDGTs

15 brGDGTs were targeted during the analysis and all compounds were detected in all samples, with brGDGT-IIIb and -IIIb', brGDGT-IIIc, brGDGT-IIc' and -IIIc' detected only in trace amounts. The summed concentrations of all brGDGTs varied from 35.6 to 3195 ng g^{-1}_{soil} (highest concentration at lowest pH values, Fig. 3a). BrGDGT-Ia is always dominant, with concentration between 9.4 and 2237 ng g^{-1}_{soil} (Fig. 3B), representing up to 84% of all brGDGTs. BrGDGT-Ia concentration varies with TOC ($r = 0.75$, $p < 0.01$, Supplementary Table S3) and pH (r =

Table 2
Soil bulk characteristics: pH*, total Organic Carbon* (TOC in %), exchangeable cations, cation exchange capacity, sum of all base cations and sum of metals. ND indicates not determined.

			%	cmolc kg^{-1}										
Date sampled	**Site #**	**pH**	**TOC**	**Al**	**Fe**	**Ca**	**K**	**Mg**	**Mn**	**Na**	**H+**	**CEC**	**Σbase**	**Σmetal**
Feb-18	1	10.5	2.0	0.000	0.000	12.2	2.0	2.5		1.2		27.6	32.7	0.000
Feb-18	2	6.5	7.0	0.000	0.001	3.9	0.4	1.0		0.2	3.1	11.5	10.4	0.002
Feb-18	3	6.0	13.5	0.008	0.003	9.7	0.4	1.6		0.3	4.5	24.6	23.3	0.033
Feb-18	4	5.4	20.0	ND	ND	ND	ND	ND	ND	ND	ND	ND	ND	ND
Feb-18	5	5.1	28.5	0.010	0.005	12.8	0.4	1.9		0.3	6.7	33.0	30.2	0.044
Feb-18	6	5.2	21.6	0.010	0.004	13.9	0.3	2.0		0.3	8.4	36.8	32.5	0.042
Feb-18	7	5.4	23.5	ND	ND	ND	ND	ND	ND	ND	ND	ND	ND	ND
Apr-18	1	9.86	2.0			15.9	1.9	2.3		1.3		35.0	39.6	0.000
Apr-18	2	6.4	6.0			5.1	0.6	1.2		0.3	2.8	13.8	13.4	0.000
Apr-18	3	5.5	17.8			14.7	0.3	2.2	0.1	0.4	9.6	39.7	34.4	0.124
Apr-18	4	5.4	21.2	0.026	0.010	14.0	0.3	2.2		0.5	10.0	38.8	33.2	0.106
Apr-18	5	5.2	32.3	0.030	0.010	20.0	0.6	2.6		0.5	11.8	53.0	46.4	0.119
Apr-18	6	5.5	22.5	0.021	0.007	19.0	1.2	2.4		0.6	10.9	50.7	44.7	0.085
Apr-18	7	5.7	27.0	0.021	0.008	16.1	0.2	2.2	0.1	0.3	8.8	41.5	37.0	0.225
Aug-18	1	10.2	1.9	0.000	0.000	12.0	2.0	0.9		1.8		27.8	29.6	0.000
Aug-18	2	9.1	3.3	0.000	0.000	13.0	0.8	1.3		0.5		27.4	29.9	0.000
Aug-18	3	6.47	5.3	0.000	0.000	3.8	0.3	1.0		0.2	3.4	11.5	10.0	0.001
Aug-18	4	6.5	5.1	0.000	0.000	3.6	0.2	0.7		0.2	4.2	11.8	8.9	0.000
Aug-18	5	6.1	7.2	0.000	0.002	3.9	0.2	0.9		0.2	2.8	11.1	10.1	0.005
Sep-18	1	9.9	9.0	0.000	0.000	16.8	1.2	2.3		1.6		36.4	40.9	0.000
Sep-18	2	8.8	35.7	0.001	0.000	19.2	1.2	3.0		0.9		40.5	46.5	0.003
Sep-18	3	6.9	16.5	0.000	0.001	5.1	0.4	1.1		0.3		10.9	13.0	0.002
Sep-18	4	6.4	3.6	0.000	0.001	2.9	0.1	0.7		0.2	3.8	10.0	7.6	0.002
Sep-18	5	6.0	22.8	0.000	0.001	3.8	0.3	0.9		0.2	3.0	11.0	9.9	0.004
Feb-19	1	9.8	2.9	0.001	0.000	16.4	1.7	1.9		1.9		36.4	40.1	0.003
Feb-19	2	5.9	7.4	0.000	0.000	2.6	0.3	0.6		0.2	3.2	8.9	7.0	0.001
Feb-19	3	5.4	6.8	0.002	0.001	3.3	0.1	0.7		0.2	2.8	9.7	8.4	0.011
Feb-19	4	5.3	15.7	0.004	0.002	11.6	0.2	1.7		0.5	3.4	27.4	27.3	0.020
Feb-19	5	5.3	12.3	0.002	0.002	7.7	0.6	1.2		0.5	3.3	19.8	19.0	0.013
Feb-19	6	4.7	34.9	ND	ND	ND	ND	ND	ND	ND	ND	ND	ND	ND
Feb-19	7	4.8	8.2	0.001	0.002	12.6	0.6	1.5	0.1	0.4	4.1	30.5	29.2	0.130
May-19	1	8.7	2.9	0.000	0.000	17.1	1.7	2.0		1.3		37.1	41.1	0.000
May-19	2	7.3	2.7	0.000	0.000	5.1	0.2	0.9		0.3	9.2	19.9	12.3	0.000
May-19	3	6.2	4.3	0.002	0.001	3.3	0.3	0.8		0.2	2.8	9.9	8.7	0.011
May-19	4	6.3	11.3	0.006	0.003	17.0	1.0	2.4		0.6	3.5	39.1	40.4	0.025
May-19	5	6.3	4.0	0.001	0.001	3.7	0.1	0.8		0.3	2.8	10.6	9.5	0.007
May-19	6	5.6	24.5	ND	ND	ND	ND	ND	ND	ND	ND	ND	ND	ND
May-19	7	6.1	3.2	0.000	0.001	1.9	0.4	0.5		0.1	3.1	7.5	5.3	0.002
Aug-20	1	9.0	3.2	0.001	0.000	17.5	1.2	2.2		1.2		37.3	41.7	0.003
Aug-20	2	6.6	4.51	0.002	0.000	3.6	1.4	0.7		0.2	3.8	12.7	10.2	0.008
Aug-20	3	6.2	5.0	0.000	0.001	2.9	0.2	0.6		0.2	3.3	9.5	7.5	0.002
Aug-20	4	5.5	5.4	0.000	0.001	4.5	0.2	1.0		0.2	2.9	12.2	11.4	0.003
Aug-20	5	5.5	4.2	0.000	0.001	2.9	0.1	0.7		0.2	3.0	9.2	7.5	0.003
Aug-20	6	5.4	10.1	0.006	0.006	11.2	0.5	1.5		0.3	4.0	27.2	26.2	0.034

*Data from Gondwe et al. (2021).
ND: Not determined.

–0.62, $p < 0.01$, Fig. 3b, Supplementary Table S3). To assess if TOC in the soils is controlling the relation between brGDGT-Ia and pH, brGDGT-Ia concentrations were normalized by TOC, and they show higher concentration in the acidic soils. This confirms that pH is one of the main factors influencing brGDGT-Ia concentrations. TOC and pH are strongly correlated with SWC (Fig. 2g), creating correlations between SWC, metal cations and free acidity and brGDGT-Ia (Supplementary Table S3).

Concentrations of brGDGT-IIa and -IIIa are also correlated with free acidity and pH, albeit less strongly than brGDGT-Ia (Fig. 3c,f, Supplementary Table S3). Concentrations of alkaline-promoted cyclopentane-containing tetramethylated brGDGT-Ib and -Ic, as well as brGDGT-IIb, are increased both at low and high pH values, resulting in a significant correlation ($0.41 < r < 0.54$, $p < 0.01$) with the concentration of exchangeable calcium and magnesium (Supplementary Table S3). A correlation with CEC ($r = 0.54$ for both, $p < 0.01$) is observed for the other 5-methyl brGDGTs with cyclopentane moieties (IIb, IIc, Supplementary Table S3). 6-methyl brGDGTs IIa' and IIIa' correlate with TOC like their 5-methyl counterparts. Their concentration increased at low pH, but also with exchangeable cations, resulting in a secondary concentration optimum at high pH (Fig. 3e,g). All 6-methyl brGDGT concentrations increase faster than their 5-methyl counterparts at high pH (Supplementary Fig. S2c). In summary, although chemical (pH, CEC) parameters control brGDGT concentrations, linear correlations do not always reflect the dependencies, as two maxima are often observed.

To describe variation in brGDGT fractional abundance, a Principal Component Analysis (PCA) is performed, calculating the loadings of brGDGTs (Fig. 4a) on two principal components. The first principal component (PC1, variation explained 60.2%) indicates the different behaviour of brGDGT-Ia and -IIa, loading oppositely to all other brGDGTs (brGDGT IIIa, Ib, Ic, IIb, IIa', IIb', IIIa'). As samples with different pH form distinct clusters (representing the three type of soils) with different PC1 scores, PC1 likely captures the influence of pH (Fig. 4a). On PC2 (explains 14.6% of the variation), soil samples with low CEC and Ca^{2+} concentrations as well as neutral pH have an increased loading. The negative loading of brGDGT-IIIa reflects an increase in the non-arid soils (Fig. 4b).

MBT'_{5ME} values, which capture variability in tetramethylated versus 5-methyl penta- and hexamethylated brGDGTs, are highly variable in the arid and non-arid soils (0.63 to 0.96) and more in the seasonally inundated soils (0.80 ± 0.05) (Supplementary Fig. S2a). MBT'_{5ME} plots positively on PC2, indicating that CEC could drive the changes in MBT'_{5ME} (Fig. 4B). CBT' varies from –1.22 to 0.02 (increasing further

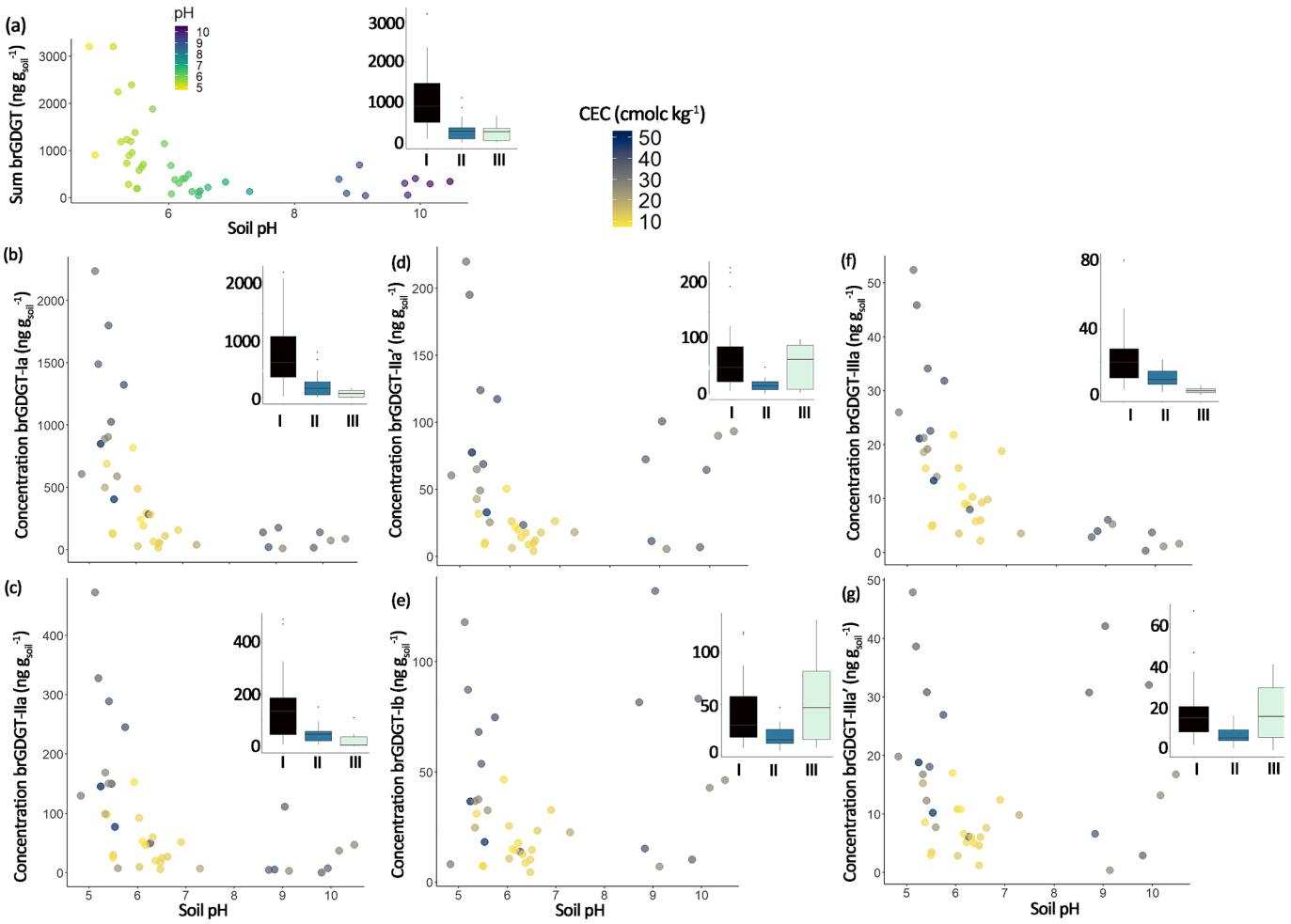

Fig. 3. Concentrations of brGDGT depending on soil pH (a) all brGDGTs, (b) brGDGT-Ia, (c) brGDGT-IIa, (d) brGDGT-IIa', (e) brGDGT-Ib, (f) brGDGT-IIIa, and (g) brGDGT-IIIa'. Color scale indicates either soil pH (panel a) or cation exchangeable capacity (panels b–g). For (a–g) average concentration of each ratio depending on soil type (I Seasonally inundated, II Non-arid, III Arid).

away from site 1; Fig. 4d). The isomer ratio (IR_{6ME}) varies from 0.1 to 0.9; values were always highest for the arid soils (site 1, 0.5 to 0.9, Fig. 4e).

3.3. isoGDGTs

IsoGDGT concentrations are in general lower (the sum of isoGDGTs is between 1.6 to 774 ng g_{soil}^{-1}, Supplementary Table S1) than brGDGT (Ri/b < 0.25). IsoGDGT-0 is the dominant isoGDGT and its concentration is lowest in the arid soils (0.6–9.8 ng g_{soil}^{-1}), increasing with distance along the transect (>150 m, 8.3–71.7 ng g_{soil}^{-1}) (Fig. 5a). IsoGDGT-0 correlates negatively with pH ($r = -0.49$, $p < 0.01$) and positively with soil water content ($r = 0.59$, $p < 0.01$) (Fig. 5b, Supplementary Table S5). Crenarchaeol and its isomer are also detected but in much lower concentration (0–81.9 ng g_{soil}^{-1}, Supplementary Table S1). The concentration of crenarchaeol correlates positively with isoGDGT-2 and -3 ($r = 0.46$, $r = 0.40$, respectively, $p < 0.01$), but not with isoGDGT-0 and -1. Crenarchaeol isomer correlates with all other isoGDGTs. The concentrations of isoGDGT-0 and isoGDGT-1, -2, -3 correlate positively ($r = 0.90$, $r = 0.84$, $r = 0.83$, $p < 0.01$, respectively, Fig. 5b, Supplementary Table S5). TEX_{86} values ranged from 0.55 to 0.97, with on average higher values for the arid soils compared with the seasonally inundated soils (sites 6 and 7; Supplementary Fig. S2g). Ri/b correlates with SWC and metal cations ($r = 0.67$ and $r = 0.54$, $p < 0.01$ respectively, Fig. 5c).

4. Discussion

4.1. Influence of aridity-driven changes in soil chemistry on brGDGTs

The succession of semi-arid, non-arid and seasonally inundated soils causes a large heterogeneity in soil chemistry. For example, the pH range of the soil covers almost the full range of the soil calibration of Dearing Crampton-Flood et al. (2020) (i.e., 3.5–8). In this context, SWC and TOC increase, whereas pH decreases with increased distance from site 1 (Fig. 1c, 2a, d), reflecting increased soil development.

4.1.1. Temperature-sensitive brGDGTs (Ia, Ib, Ic, IIa, IIb, IIc, IIIa)

In the Okavango Delta soils studied here, MAST temperature values fall within a narrow 2 °C range. Therefore, the large variations seen in brGDGTs and brGDGT proxies cannot be driven by temperature changes. BrGDGT-Ia, -IIa and -IIIa concentrations correlate negatively with pH (Fig. 3b,c,f), indicating that in absence of temperature variation these temperature-dependent brGDGTs are controlled by pH changes. The concentrations of other proposed temperature-dependent brGDGTs: brGDGT-Ib, and -IIb correlate with exchangeable cations and CEC (Supplementary Table S3), as observed by Halffman et al. (2022) in Swedish soils, and De Jonge et al. (2024) in soils from six globally distributed elevation transects.

These parameters have a clear impact on MBT'_{5ME}, which shows a large range of values (0.63 to 0.96) which equates to almost 10 °C of reconstructed MAAT using [Eq. (6)] (19–29 °C, Fig. 4c). However, this

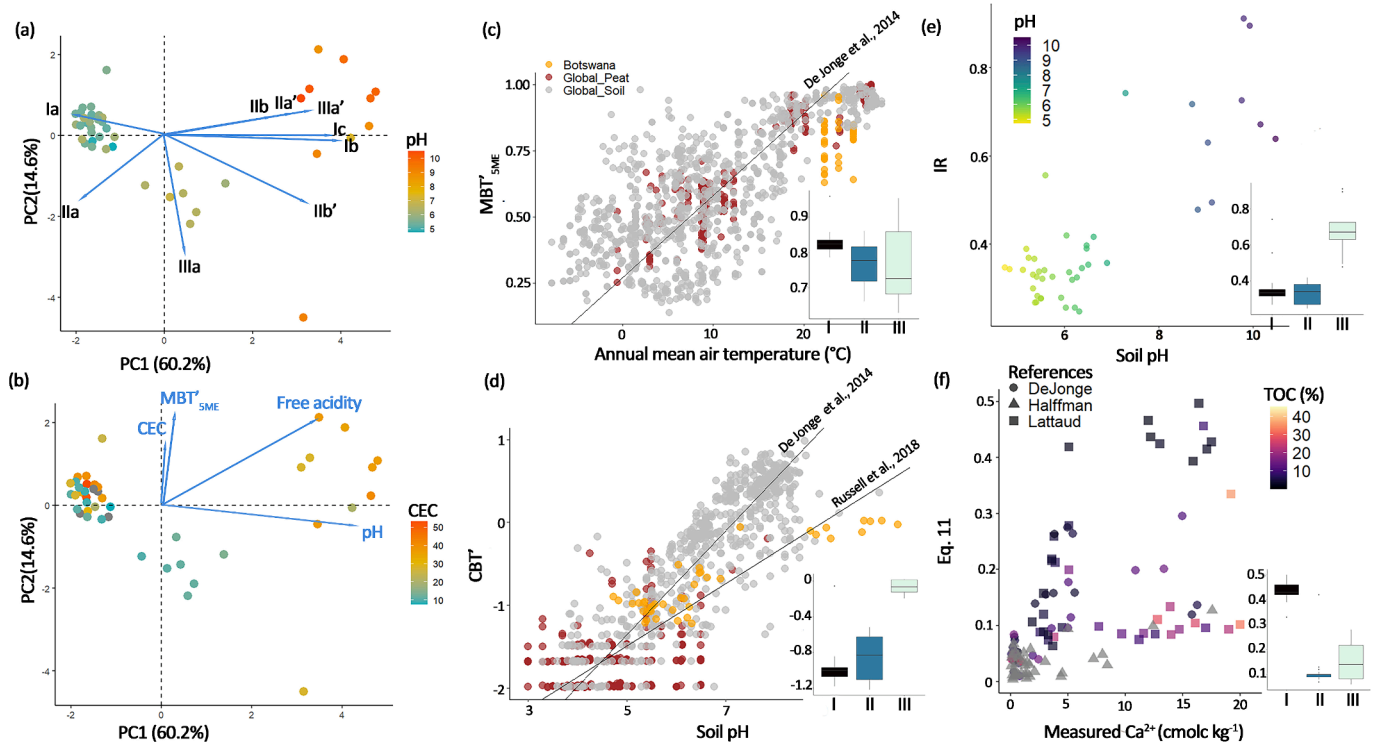

Fig. 4. (a, b) PCA of standardized fractional brGDGT abundances, with brGDGT fractional abundances (a) and MBT'$_{5ME}$ ratio values and environmental parameters (b) plotted a posteriori. Symbol colors refer to either (a) pH and (b) or CEC (in cmolc kg^{-1}). (c) MBT'$_{5ME}$ values of globally distributed soils and peats, plotted against annual mean air temperature, (d) CBT' values of globally distributed soils and peats plotted against soil pH. For (c,d) Botswana soils analysed in this study are plotted with orange symbols. In panel (c) the calibration line between MBT'$_{5ME}$ and MAAT of De Jonge et al (2014a) is plotted, panel d) includes both the calibrations of Russell et al. (2018) and De Jonge et al. (2014a). (e) Isomer ratio (IR) and soil pH and (f) brGDGT-based ratio [Eq. 11] from De Jonge et al. (2024) plotted against the measured concentration in exchangeable calcium. Data from the Okavango Delta (this study), De Jonge et al. (2024) and Halffman et al. (2022). For (c–f) average values of each ratio depending on soil type (I Seasonally inundated, II Non arid, III Arid).

does not result in a correlation between MBT'$_{5ME}$ and pH (Supplementary Fig. S2b), contrary to what is reported by Halffman et al. (2022). Previous studies have shown that arid (alkaline) and non-arid (acidic) soils have MBT'$_{5ME}$ with different relationships to environmental parameters (Guo et al., 2022). Indeed, when arid (alkaline, pH>8) soils are separated from the non-arid and seasonally inundated soils (acidic, pH<6), the latter (n = 33) show a negative relationship between pH and MBT'$_{5ME}$ ($r = -0.59$, $p < 0.01$, Supplementary Fig. S2b), similar to Halffman et al. (2022). On the other hand, in the arid soils (n = 10) no dependency between MBT'$_{5ME}$ and pH is observed, instead MBT'$_{5ME}$ correlates with IR$_{6ME}$ ($r = 0.98$, $p < 0.01$, Supplementary Table S4b). A first difference between these types of soils is the faster increase in the fractional abundance in brGDGT-IIa', in parallel with higher amount of brGDGT-Ib in arid soils compared with seasonally inundated soils, maybe due to the presence of a different community of producers (Supplementary Fig. S2c, d). A second source of variation in the MBT'$_{5ME}$ values in non-arid soils, is caused by the increased fractional abundance of brGDGT IIIa in soils with neutral pH (i.e., the non-arid soils, Fig. 4b, Supplementary Fig. S2e). Here, variations in MBT'$_{5ME}$ could be explained by: (i) an allochthonous source of brGDGT-IIIa, brought by the river, especially in the seasonally flooded soils (hypothesis I), or (ii) an additional control by CEC (hypothesis II) (Fig. 4b). In support of hypothesis I, the concentration of brGDGT-IIIa increases in water-logged soils, but its fractional abundance is only slightly different (Supplementary Fig. S2e). The concentration increases seen in brGDGT-IIIa thus likely reflect the increase observed for all brGDGTs and not an influence of the nearby river (Fig. 3a). In addition, the ratio of brGDGT-IIIa over -IIa (Xiao et al., 2016) is below the reported threshold for lacustrine production (0.9, Martin et al., 2019) in all but two soil samples that have SWC<25 %. However, due to the lack of end-member data for the riverine brGDGTs, the use of the IIIa over IIa ratio is uncertain (O'Beirne et al., 2024). Indeed, here, higher IIIa versus IIa ratios are found at lower SWC (<25 %) and higher MBT'$_{5ME}$ (Supplementary Fig. S2f). In conclusion, as no strong support is present for hypothesis I, MBT'$_{5ME}$ variations are likely due to variation in CEC that impacts the production of brGDGT-IIIa in neutral pH soils (hypothesis II), a hitherto unknown and poorly constrained confounding factor for MBT'$_{5ME}$ in the non-inundated, non-arid soils.

4.1.2. *Alkalinity-promoted brGDGTs (6-methyl and cyclopentane-containing brGDGTs)*

In the seasonally inundated soils, high CEC, driven by Ca^{2+} and low pH, are likely caused by plant evapotranspiration precipitating Ca^{2+} (Ellery et al., 1993; Milzow et al., 2009). In the semi-arid alkaline soils, Ca^{2+}concentrations are also increased, likely caused by the extreme evaporation in these soils. Hence, there is no correlation between pH and CEC (or Ca^{2+}), as such this is the ideal dataset to test the effect of CEC independently of pH.

The summed brGDGTs concentration is higher in low pH (<6) than in higher pH soils (>9, Fig. 3a), which is driven by an increase in brGDGT-Ia, -IIa, -IIIa (Fig. 3b,c,f) and in agreement with previous studies (e.g., Peterse et al., 2010; De Jonge et al., 2019). This increase is likely due to the increased abundance of potential brGDGT producers such as Acidobacteria in low pH soils (Jones et al., 2009). All other brGDGTs show two optima, with higher concentration in both low pH and high pH soils (Fig. 3d,e,g), indicating additional production or different brGDGT producers at higher pH, potentially Actinobacteria and Verrucomicrobia (e.g, Guo et al., 2022).

The concentrations of the 6-methyl brGDGTs (IIa', IIIa') and cyclopentane-containing brGDGTs (Ib, IIb, IIc, IIIb) correlate positively

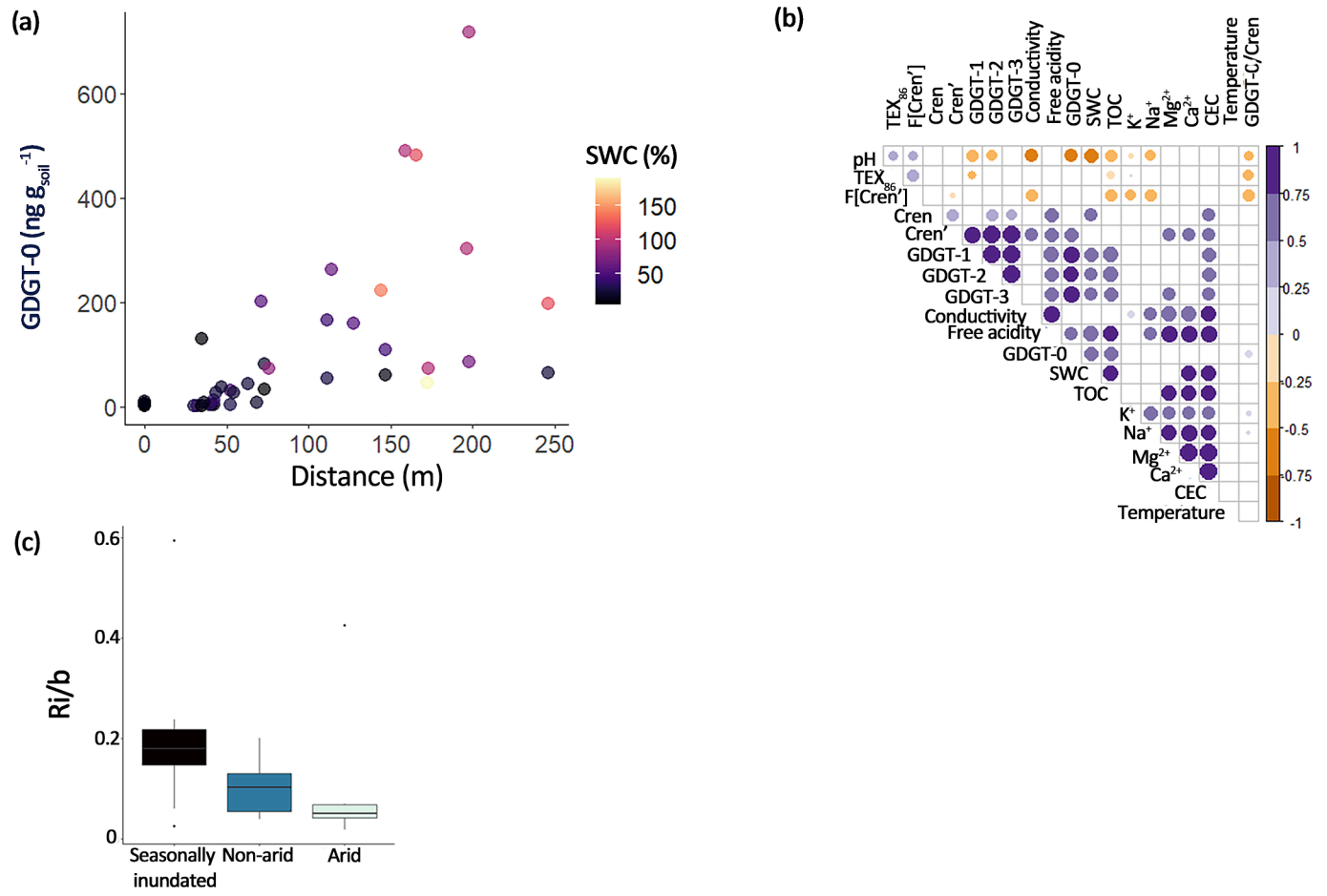

Fig. 5. (a) Concentration of GDGT-0 (ng g_{soil}^{-1}) along the sampling transect (distance from Site 1 in m); the color scheme indicates soil water content (SWC). (b) Correlation matrix between the concentration of isoGDGTs and isoGDGT-based ratios and environmental parameters (only significant correlations, i.e. with $p < 0.01$ are indicated with coloured circles which size is proportional to their Pearson r). Coefficients are provided in Supplementary Table S5. (c) The ratio of isoprenoid versus branched GDGT depending on soil type.

with CEC and exchangeable Ca^{2+} ($0.54<r<0.58$, Fig. 3d,g, Supplementary Table S3), which is similar to what was reported by Halffman et al. (2022) and De Jonge et al. (2021, 2024) in very different settings (temperate, arid, and tropical sites). This confirms the impact of CEC on alkalinity-promoted brGDGTs, even in the absence of a temperature change. For the arid alkaline soils there is a higher abundance of the 6-methyl brGDGTs (IIa', IIIa') compared with their 5-methyl counterpart (IIa, IIIa), which results in high IR_{6ME} values (0.5–0.9, Fig. 4e). In contrast, 5-methyl brGDGTs dominate their 6-methyl counterparts at wetter sites. This is in agreement with previous studies of alkaline soils (pH>8) in several regions of the globe where 97% of IR_{6ME} values are > 0.5 (De Jonge et al., 2014a, 2014b; Dang et al., 2016a; Dang et al., 2016b; Ding et al., 2016; Wang et al., 2016; Xiao et al., 2016; Duan et al., 2020, 2022; Dearing Crampton-Flood et al., 2020; Pérez-Angel et al., 2020; Chen et al., 2021; Guo et al., 2022; Peaple et al., 2022). IR_{6ME} is positively correlated with pH (Fig. 4e), the main exchangeable cations (Ca^{2+}, Mg^{2+}, K^+, Na^+) and conductivity, albeit with a low correlation factor ($r < 0.19$ for EC, $p < 0.01$, Supplementary Table S4). CBT' only responds to pH ($r = 0.63$, $p < 0.01$, Fig. 4D), and only weakly to Na^+ ($r = -0.18$, $p < 0.01$), confirming its use as a pH proxy.

Alkalinity-promoted brGDGTs (Ib, IIa', IIb') increase with increasing exchangeable Ca^{2+} (Supplementary Table S3). As such [Eq. 11] from De Jonge et al. (2024) was calculated and compared with the concentration in exchangeable Ca^{2+}. The ratio reconstructs Ca^{2+} concentration accurately for some soils but performed badly for others (Fig. 4f). The only parameter that can predict the efficiency of Eq. 11 to reconstruct the concentration in Ca^{2+} is TOC content. Soil samples with TOC < 15% accurately reflected the concentration in Ca^{2+} (Fig. 4f). Hence, at this location, reconstructing Ca^{2+} using brGDGTs is possible but should be limited to soil with TOC < 15%. Even with this limitation, this makes this new ratio a potential proxy to reconstruct past concentration in exchangeable calcium, potentially accessing past soil conductivity.

4.2. Environmental drivers of isoGDGT distribution

The correlation between CEC, free acidity and the concentration of isoGDGT-1, -2, -3 (Fig. 5b, Supplementary Table S5) can be linked to the increased membrane impermeability to protons thanks to the presence of cyclopentane rings (Dannenmuller et al., 2000; Caforio and Driessen, 2017).

Archaeal community change is likely at the base of these correlation differences, i.e., there likely is a common Thaumarchaeota producer(s) for isoGDGT-1, -2, -3, and crenarchaeol (and crenarchaeol isomer), and an additional one for isoGDGT-0 (which can have multiple sources, e.g., Schouten et al., 2013). The pH has been reported to be the main control on archaeal diversity in tropical soils (Tripathi et al., 2013). For crenarchaeol, a marker for the ammonia oxidizing Thaumarchaeota (Pester et al., 2011), Blewett et al. (2020) reported an increased concentration of crenarchaeol in dry wetlands with neutral pore water pH (pH=6.8), compared to more humid and acid wetlands. However, in our dataset, crenarchaeol concentration does not correlate with pH but with CEC and free acidity, and it is more abundant in wetter soil with neutral to acidic pH (5<pH<7). This might come from the increased abundance of ammonia oxidizing Thaumarchaeota in the water-logged soils during

the high flood season, while during the low flood season crenarchaeol is more abundant in the driest soil. In the alkaline soils from Botswana, it is likely that Thaumarchaeota group 1.1b dominates the archaeal assemblages (as the soils show an increase in the proportion of crenarchaeol isomer, Supplementary Fig. S2h, Dirghangi et al., 2013; Baxter et al., 2021), while the more acidic soils could show a larger diversity of thaumarchaeotal groups (Tripathi et al., 2013). However, 16S DNA sequencing would be needed to confirm this hypothesis. There is no increased concentration in isoGDGTs in the dry soils, to the contrary of what Pei et al. (2021) showed, likely coming from difference in mineralogy in both sets of soils, i.e. the dry Botswana soils are arenosols and do not contains a lot of clay (85% sand, Gondwe et al., 2021). Clays are minerals that can easily bind organic matter (Blair and Aller, 2012), and isoGDGTs, and preserve them over long periods of time (Freymond et al., 2018; Gies et al., 2021, 2023).

For isoGDGT-0, a dominant methanogenic Euryarchaeota source is plausible in the seasonally inundated soils, as these soils are high in organic matter and seasonally anoxic. In addition, relatively high methane fluxes have been reported from this part of the transect (Gondwe et al., 2021). When testing the ratio of isoGDGT-0 over crenarchaeol (Supplementary Table S2), potentially indicative of methanogens in lacustrine systems (Blaga et al., 2009), the ratio is above 2 for all except the arid soils, reflecting the confirmed presence of methanogens throughout the transect (Gondwe et al., 2021). The concentration of isoGDGT-0 in the arid soils is lower than in the other types of soils, which is linked to higher pH and low SWC (Fig. 5a). This is in agreement with an observed decrease of archaeal abundance in tropical soils with higher pH (Tripathi et al., 2013).

The ratio of isoprenoid versus branched GDGTs correlates with soil water content ($r = 0.45$, $p < 0.01$, Fig. 5c), indicating that this proxy developed by Xie et al. (2012) can track moisture changes along a transect of seasonally inundated to arid soils, with the distinction that here it tracks river moisture, and not precipitation. There is no mean annual soil temperature variation, hence the variations in TEX_{86} are explained by other environmental parameters. TEX_{86} correlate positively with pH ($r = 0.63$, $p < 0.01$, Supplementary Fig. S2g), which can be driver of archaeal community change. Hence, the use of TEX_{86} to reconstruct temperature can be biased by pH-driven archaeal community change and should be used with caution.

5. Conclusions

Branched and isoprenoid GDGT concentration and distribution changes were studied in 43 soil samples in a seasonal floodplain in the Okavango Delta (Botswana). This allowed for a clear study of the effect of aridity-driven soil chemistry on branched and isoGDGT distributions, independent of temperature variations. When correlating alkalinity-promoted brGDGT concentrations with soil pH, linear correlations were not suited as the concentration (normalized per g soil) of the brGDGTs (i.e., IIa', IIIa', Ib, Ic, IIb, IIb') increased both at low and high pH, correlating linearly with exchangeable Mg^{2+}, Ca^{2+} and CEC instead. Overall MBT'_{5ME} is driven by changes in CEC; in addition, in non-arid soils, MBT'_{5ME} correlates with pH. In arid soils, MBT'_{5ME} correlates with IR_{6ME}. Hence, a change from arid to non-arid soil can potentially impact temperature reconstruction using the MBT'_{5ME}. CBT' correlates only with pH and remains a valuable proxy for soil pH reconstructions. Reconstructing the concentration of exchangeable Ca^{2+} can be attempted successfully in low TOC soils, using Eq. 11 developed by De Jonge et al. (2024). The concentration of isoGDGT-0 responded to changes in pH, free acidity and soil water content, in agreement with a likely production by methanogenic Euryarchaeota in seasonally inundated soils. TEX_{86} is positively correlated with increasing pH and reflects the impact of pH on archaeal diversity. The Ri/b ratio correlates with soil water content across the whole soil moisture gradient, as shown in previous studies, and highlights the potential for this ratio to be used in geological setting to reconstruct soil moisture content, even when it is controlled by seasonal river flooding. In similar settings to the Okavango Delta such as loess deposits, these confounding factors on the MBT'_{5ME} should be considered. BrGDGTs could be reliable tracers of exchangeable cation capacity. In addition, with some more calibration work, they could also be used to trace exchangeable Ca^{2+}.

CRediT authorship contribution statement

Julie Lattaud: Writing – original draft, Visualization, Project administration, Methodology, Investigation, Conceptualization. **Mangaliso J. Gondwe:** Writing – review & editing, Resources. **Marco Griepentrog:** Writing – review & editing, Resources, Methodology. **Carole Helfter:** Writing – review & editing, Resources. **Cindy De Jonge:** Writing – review & editing, Methodology, Funding acquisition.

Declaration of competing interest

The authors declare that they have no known competing financial interests or personal relationships that could have appeared to influence the work reported in this paper.

Data availability

The data are in an open online repository, the link is shared in the article

Acknowledgments

We thank the associate editor John Volkman, and three anonymous reviewers for their time reviewing this manuscript. We thank Mr. T. Kemosedile and Mr. E. Kambato, field technicians of the Okavango Research Institute that assisted during the campaigns. The soil samples used in this paper were collected under a research project funded by the UK Natural Environment Research Council under grant nos. NE/N015746/1 and NE/N015746/2, and conducted under research permit EWT 8/36/4 XXXI [18] from the Botswana Ministry of Environment, Natural Resources Conservation and Tourism. J. Lattaud was funded by an ETH commission grant (OKAPI, ETH 2020-1) to C. De Jonge. The dataset is available on the ETHZ data repository: https://doi.org/10.3929/ethz-b-000669918.

References

Auguet, J.-C., Barberan, A., Casamayor, E.O., 2010. Global ecological patterns in uncultured Archaea. The ISME Journal 4, 182–190.
Bates, S.T., Berg-Lyons, D., Caporaso, J.G., Walters, W.A., Knight, R., Fierer, N., 2011. Examining the global distribution of dominant archaeal populations in soil. The ISME Journal 5, 908–917.
Baxter, A.J., van Bree, L.G.J., Peterse, F., Hopmans, E.C., Villanueva, L., Verschuren, D., Sinninghe Damsté, J.S., 2021. Seasonal and multi-annual variation in the abundance of isoprenoid GDGT membrane lipids and their producers in the water column of a meromictic equatorial crater lake (Lake Chala, East Africa). Quaternary Science Reviews 273, 107263.
Blaga, C.I., Reichart, G.J., Heiri, O., Sinninghe Damsté, J.S., 2009. Tetraether membrane lipid distributions in water-column particulate matter and sediments: A study of 47 European lakes along a north-south transect. Journal of Paleolimnology 41, 523–540.
Blair, N.E., Aller, R.C., 2012. The Fate of Terrestrial Organic Carbon in the Marine Environment. Annual Review of Marine Science 4, 401–423.
Blewett, J., Naafs, B.D.A., Gallego-Sala, A.V., Pancost, R.D., 2020. Effects of temperature and pH on archaeal membrane lipid distributions in freshwater wetlands. Organic Geochemistry 148, 104080.
Brown, I.C., 1943. A rapid method of determining exchangeale hydrogen and total exchangeable bases of soils. Soil Science 56, 353.
Caforio, A., Driessen, A.J.M., 2017. Archaeal phospholipids: Structural properties and biosynthesis. Biochimica et Biophysica Acta (BBA) - Molecular and Cell Biology of Lipids. Bacterial Lipids 1862, 1325–1339.
Chen, C., Bai, Y., Fang, X., Zhuang, G., Khodzhiev, A., Bai, X., Murodov, A., 2021. Evaluating the potential of soil bacterial tetraether proxies in westerlies dominating western Pamirs, Tajikistan and implications for paleoenvironmental reconstructions. Chemical Geology 559, 119908.
Chen, Y., Zheng, F., Yang, H., Yang, W., Wu, R., Liu, X., Liang, H., Chen, H., Pei, H., Zhang, C., Pancost, R.D., Zeng, Z., 2022. The production of diverse brGDGTs by an

Acidobacterium providing a physiological basis for paleoclimate proxies. Geochimica et Cosmochimica Acta 337, 155–165.
Coffinet, S., Huguet, A., Williamson, D., Fosse, C., Derenne, S., 2014. Potential of GDGTs as a temperature proxy along an altitudinal transect at Mount Rungwe (Tanzania). Organic Geochemistry 68, 82–89.
Dang, X., Yang, H., Naafs, B.D.A., Pancost, R.D., Xie, S., 2016a. Evidence of moisture control on the methylation of branched glycerol dialkyl glycerol tetraethers in semi-arid and arid soils. Geochimica et Cosmochimica Acta 189, 24–36.
Dang, X.Y., Xue, J.T., Yang, H., Xie, S.C., 2016b. Environmental impacts on the distribution of microbial tetraether lipids in Chinese lakes with contrasting pH: Implications for lacustrine paleoenvironmental reconstructions. Science China Earth Sciences 59, 939–950.
Dannenmuller, O., Arakawa, K., Eguchi, T., Kakinuma, K., Blanc, S., Albrecht, A.-M., Schmutz, M., Nakatani, Y., Ourisson, G., 2000. Membrane Properties of Archæal Macrocyclic Diether Phospholipids. Chemistry – A. European Journal 6, 645–654.
Davtian, N., Ménot, G., Bard, E., Poulenard, J., Podwojewski, P., 2016. Consideration of soil types for the calibration of molecular proxies for soil pH and temperature using global soil datasets and Vietnamese soil profiles. Organic Geochemistry 101, 140–153.
De Jonge, C., Hopmans, E.C., Zell, C.I., Kim, J.-H.-H., Schouten, S., Sinninghe Damsté, J. S., Jonge, C.D., Hopmans, E.C., Zell, C.I., Kim, J.-H.-H., Schouten, S., Damsté, J.S.S., 2014a. Occurrence and abundance of 6-methyl branched glycerol dialkyl glycerol tetraethers in soils: implications for palaeoclimate reconstruction. Geochimica et Cosmochimica Acta 141, 97–112.
De Jonge, C., Stadnitskaia, A., Hopmans, E.C., Cherkashov, G., Fedotov, A., Sinninghe Damsté, J.S., 2014b. In situ produced branched glycerol dialkyl glycerol tetraethers in suspended particulate matter from the Yenisei River, Eastern Siberia. Geochimica et Cosmochimica Acta 125, 476–491.
De Jonge, C., Radujković, D., Sigurdsson, B.D., Weedon, J.T., Janssens, I., Peterse, F., 2019. Lipid biomarker temperature proxy responds to abrupt shift in the bacterial community composition in geothermally heated soils. Organic Geochemistry 137, 103897.
De Jonge, C., Kuramae, E.E., Radujković, D., Weedon, J.T., Janssens, I.A., Peterse, F., 2021. The influence of soil chemistry on branched tetraether lipids in mid- and high latitude soils: Implications for brGDGT- based paleothermometry. Geochimica et Cosmochimica Acta 310, 95–112.
De Jonge, C., Guo, J., Hällberg, P., Griepentrog, M., Rifai, H., Richter, A., Ramirez, E., Zhang, X., Smittenberg, R.H., Peterse, F., Boeckx, P., Dercon, G., 2024. The impact of soil chemistry, moisture and temperature on branched and isoprenoid GDGTs in soils: A study using six globally distributed elevation transects. Organic Geochemistry 187, 104706.
Dearing Crampton-Flood, E., Tierney, J.E., Peterse, F., Kirkels, F.M.S.A., Sinninghe Damsté, J.S., 2020. BayMBT: A Bayesian calibration model for branched glycerol dialkyl glycerol tetraethers in soils and peats. Geochimica et Cosmochimica Acta 268, 142–159.
Ding, S., Schwab, V.F., Ueberschaar, N., Roth, V.N., Lange, M., Xu, Y., Gleixner, G., Pohnert, G., 2016. Identification of novel 7-methyl and cyclopentanyl branched glycerol dialkyl glycerol tetraethers in lake sediments. Organic Geochemistry 102. https://doi.org/10.1016/j.orggeochem.2016.09.009.
Dirghangi, S.S., Pagani, M., Hren, M.T., Tipple, B.J., 2013. Distribution of glycerol dialkyl glycerol tetraethers in soils from two environmental transects in the USA. Organic Geochemistry 59, 49–60.
Duan, Y., Sun, Q., Werne, J.P., Yang, H., Jia, J., Wang, L., Xie, H., Chen, F., 2020. Soil pH Dominates the Distributions of Both 5- and 6-Methyl Branched Tetraethers in Arid Regions. Journal of Geophysical Research: Biogeosciences 125, e2019JG005356.
Duan, Y., Sun, Q., Werne, J.P., Hou, J., Yang, H., Wang, Q., Khormali, F., Chen, F., 2022. The impact of precipitation on the distributions of branched tetraethers in alkaline soils. Organic Geochemistry 169, 104410.
Dugerdil, L., Joannin, S., Peyron, O., Jouffroy-Bapicot, I., Vannière, B., Boldgiv, B., Unkelbach, J., Behling, H., Ménot, G., 2021. Climate reconstructions based on GDGT and pollen surface datasets from Mongolia and Baikal area: calibrations and applicability to extremely cold–dry environments over the Late Holocene. Climate of the Past 17, 1199–1226.
Ellery, W.N., Ellery, K., McCarthy, T.S., 1993. Plant distribution in islands of the Okavango Delta, Botswana: determinants and feedback interactions. African Journal of Ecology 31, 118–134.
Freymond, C.V., Kündig, N., Stark, C., Peterse, F., Buggle, B., Lupker, M., Plötze, M., Blattmann, T.M., Filip, F., Giosan, L., Eglinton, T.I., 2018. Evolution of biomolecular loadings along a major river system. Geochimica et Cosmochimica Acta 223, 389–404.
Gies, H., Hagedorn, F., Lupker, M., Montluçon, D., Haghipour, N., Van Der Voort, T.S., Eglinton, T.I., 2021. Millennial-age glycerol dialkyl glycerol tetraethers (GDGTs) in forested mineral soils: ^{14}C-based evidence for stabilization of microbial necromass. Biogeosciences 18, 189–205.
Gies, H., Lupker, M., Galy, V., Hemingway, J., Boehman, B., Schwab, M., Haghipour, N., Eglinton, T.I., 2023. Multi-molecular 14C evidence for mineral control on terrestrial carbon storage and export. Philosophical Transactions of the Royal Society A, Mathematical, Physical, and Engineering Sciences 381, 20220328.
Gondwe, M.J., Helfter, C., Murray-Hudson, M., Levy, P.E., Mosimanyana, E., Makati, A., Mfundisi, K.B., Skiba, U.M., 2021. Methane flux measurements along a floodplain soil moisture gradient in the Okavango Delta, Botswana. Philosophical Transactions of the Royal Society A, Mathematical, Physical, and Engineering Sciences 379. https://doi.org/10.1098/rsta.2020.0448.
Gumbricht, T., McCarthy, J., McCarthy, T.S., 2004a. Channels, wetlands and islands in the Okavango Delta, Botswana, and their relation to hydrological and sedimentological processes. Earth Surface Processes and Landforms 29, 15–29.
Gumbricht, T., Wolski, P., Frost, P., McCarthy, T.S., 2004b. Forecasting the spatial extent of the annual flood in the Okavango delta, Botswana. Journal of Hydrology 290, 178–191.
Guo, H., Cao, Y., Wei, S., Shi, F., Jia, G., Haokun, B., Zhaoyan, G.U., Zhiguo, R., a. O.,, 2021. Integrated investigation of GDGTs in surface soils and peat sediments in the southern Altai Mountains in arid Central Asia. Quaternary Sciences 41, 1069–1093.
Guo, J., Ma, T., Liu, N., Zhang, X., Hu, H., Ma, W., Wang, Z., Feng, X., Peterse, F., 2022. Soil pH and aridity influence distributions of branched tetraether lipids in grassland soils along an aridity transect. Organic Geochemistry 164, 104347.
Häggi, C., Naafs, B.D.A., Silvestro, D., Bertassoli, D.J., Akabane, T.K., Mendes, V.R., Sawakuchi, A.O., Chiessi, C.M., Jaramillo, C.A., Feakins, S.J., 2023. GDGT distribution in tropical soils and its potential as a terrestrial paleothermometer revealed by Bayesian deep-learning models. Geochimica et Cosmochimica Acta 362, 41–64.
Halamka, McFarlin, J.M., Younkin, A.D., Depoy, J., Dildar, N., Kopf, S., 2021. Oxygen limitation can trigger the production of branched GDGTs in culture. Geochemical Perspectives Letters 19. https://doi.org/10.7185/geochemlet.2132.
Halamka, T.A., Raberg, J.H., McFarlin, J.M., Younkin, A.D., Mulligan, C., Liu, X.-L., Kopf, S.H., 2023. Production of diverse brGDGTs by Acidobacterium Solibacter usitatus in response to temperature, pH, and O_2 provides a culturing perspective on brGDGT proxies and biosynthesis. Geobiology 21, 102–118.
Halffman, R., Lembrechts, J., Radujković, D., De Gruyter, J., Nijs, I., De Jonge, C., 2022. Soil chemistry, temperature and bacterial community composition drive brGDGT distributions along a subarctic elevation gradient. Organic Geochemistry 163, 104346.
Hopmans, E.C., Schouten, S., Sinninghe Damsté, J.S., 2016. The effect of improved chromatography on GDGT-based palaeoproxies. Organic Geochemistry 93, 1–6.
Huguet, C., Hopmans, E.C., Febo-Ayala, W., Thompson, D.H., Sinninghe Damsté, J.S., Schouten, S., 2006. An improved method to determine the absolute abundance of glycerol dibiphytanyl glycerol tetraether lipids. Organic Geochemistry 37, 1036–1041.
Jaeschke, A., Rethemeyer, J., Lappé, M., Schouten, S., Boeckx, P., Schefuß, E., 2018. Influence of land use on distribution of soil n-alkane δD and brGDGTs along an altitudinal transect in Ethiopia: Implications for (paleo)environmental studies. Organic Geochemistry 124, 77–87.
Jones, R.T., Robeson, M.S., Lauber, C.L., Hamady, M., Knight, R., Fierer, N., 2009. A comprehensive survey of soil acidobacterial diversity using pyrosequencing and clone library analyses. The ISME Journal 3, 442–453.
Kassambara, A., Mundt, F., n.d. factoextra : Extract and Visualize the Results of Multivariate Data Analyses.Retrieved April 13, 2023, from https://rpkgs.datanovia.com/factoextra/index.html.
Lattaud, J., Bröder, L., Haghipour, N., Rickli, J., Giosan, L., Eglinton, T.I., 2021. Influence of Hydraulic Connectivity on Carbon Burial Efficiency in Mackenzie Delta Lake Sediments. Journal of Geophysical Research: Biogeosciences 126. https://doi.org/10.1029/2020jg006054.
Lê, S., Josse, J., Husson, F., 2008. FactoMineR: An R Package for Multivariate Analysis. Journal of Statistical Software 25, 1–18.
Li, Y., Zhao, S., Pei, H., Qian, S., Zang, J., Dang, X., Yang, H., 2018. Distribution of glycerol dialkyl glycerol tetraethers in surface soils along an altitudinal transect at cold and humid Mountain Changbai: Implications for the reconstruction of paleoaltimetry and paleoclimate. Science China Earth Sciences 61, 925–939.
Loomis, S.E., Russell, J.M., Sinninghe Damsté, J.S., 2011. Distributions of branched GDGTs in soils and lake sediments from western Uganda: Implications for a lacustrine paleothermometer. Organic Geochemistry 42, 739–751.
Martin, C., Ménot, G., Thouveny, N., Davtian, N., Andrieu-Ponel, V., Reille, M., Bard, E., 2019. Impact of human activities and vegetation changes on the tetraether sources in Lake St Front (Massif Central, France). Organic Geochemistry 135, 38–52.
Menges, J., Huguet, C., Alcañiz, J.M., Fietz, S., Sachse, D., Rosell-Melé, A., 2014. Influence of water availability in the distributions of branched glycerol dialkyl glycerol tetraether in soils of the Iberian Peninsula. Biogeosciences 11, 2571–2581.
Milzow, C., Kgotlhang, L., Bauer-Gottwein, P., Meier, P., Kinzelbach, W., 2009. Regional review: the hydrology of the Okavango Delta, Botswana—processes, data and modelling. Hydrogeology Journal 17, 1297–1328.
Naafs, B.D.A., Inglis, G.N., Zheng, Y., Amesbury, M.J., Biester, H., Bindler, R., Blewett, J., Burrows, M.A., del Castillo Torres, D., Chambers, F.M., Cohen, A.D., Evershed, R.P., Feakins, S.J., Gałka, M., Gallego-Sala, A., Gandois, L., Gray, D.M., Hatcher, P.G., Honorio Coronado, E.N., Hughes, P.D.M., Huguet, A., Könönen, M., Laggoun-Défarge, F., Lähteenoja, O., Lamentowicz, M., Marchant, R., McClymont, E., Pontevedra-Pombal, X., Ponton, C., Pourmand, A., Rizzuti, A.M., Rochefort, L., Schellekens, J., De Vleeschouwer, F., Pancost, R.D., 2017. Introducing global peat-specific temperature and pH calibrations based on brGDGT bacterial lipids. Geochimica et Cosmochimica Acta 208, 285–301.
O'Beirne, M.D., Scott, W.P., Contreras, S., Araneda, A., Tejos, E., Moscoso, J., Werne, J. P., 2024. Distribution of branched glycerol dialkyl glycerol tetraether (brGDGT) lipids from soils and sediments from the same watershed are distinct regionally (central Chile) but not globally. Frontiers in Earth Science 12. https://doi.org/10.3389/feart.2024.1383146.
Peaple, M.D., Beverly, E.J., Garza, B., Baker, S., Levin, N.E., Tierney, J.E., Häggi, C., Feakins, S.J., 2022. Identifying the drivers of GDGT distributions in alkaline soil profiles within the Serengeti ecosystem. Organic Geochemistry 169, 104433.
Pei, H., Zhao, S., Yang, H., Xie, S., 2021. Variation of branched tetraethers with soil depth in relation to non-temperature factors: Implications for paleoclimate reconstruction. Chemical Geology 572, 120211.
Pérez-Angel, L.C., Sepúlveda, J., Molnar, P., Montes, C., Rajagopalan, B., Snell, K., Gonzalez-Arango, C., Dildar, N., 2020. Soil and Air Temperature Calibrations Using

Branched GDGTs for the Tropical Andes of Colombia: Toward a Pan-Tropical Calibration. Geochemistry, Geophysics, Geosystems 21.
Pester, M., Schleper, C., Wagner, M., 2011. The Thaumarchaeota: an emerging view of their phylogeny and ecophysiology. Current Opinion in Microbiology, Ecology and Industrial Microbiology / Special Section: Archaea 14, 300–306.
Peterse, F., Nicol, G.W., Schouten, S., Sinninghe Damsté, J.S., 2010. Influence of soil pH on the abundance and distribution of core and intact polar lipid-derived branched GDGTs in soil. Organic Geochemistry 41, 1171–1175.
R Core Team, 2023. R: A Language and Environment for Statistical Computing [Computer software]. R Foundation for Statistical Computing. https://www.R-project.org/.
Schouten, S., Hopmans, E.C., Sinninghe Damsté, J.S., 2002. Distributional variations in marine crenarchaeotal membrane lipids: a new tool for reconstructing ancient sea water temperatures? Earth and Planetary Science Letters 204, 265–274.
Schouten, S., Hopmans, E.C., Sinninghe Damsté, J.S., 2013. The organic geochemistry of glycerol dialkyl glycerol tetraether lipids: A review. Organic Geochemistry 54, 19–61.
Sinninghe Damsté, J.S., Schouten, S., Hopmans, E.C., van Duin, A.C.T., Geenevasen, J.A. J., 2002. Crenarchaeol. Journal of Lipid Research 43, 1641–1651.
Sinninghe Damsté, J.S., Rijpstra, W.I.C., Hopmans, E.C., Weijers, J.W.H., Foesel, B.U., Overmann, J., Dedysh, S.N., 2011. 13,16-Dimethyl Octacosanedioic Acid (iso-Diabolic Acid), a Common Membrane-Spanning Lipid of Acidobacteria Subdivisions 1 and 3. Applied and Environmental Microbiology 77, 4147–4154.
Slessarev, E.W., Lin, Y., Bingham, N.L., Johnson, J.E., Dai, Y., Schimel, J.P., Chadwick, O. A., 2016. Water balance creates a threshold in soil pH at the global scale. Nature 540, 567–569.
Tripathi, B.M., Kim, M., Lai-Hoe, A., Shukor, N.A.A., Rahim, R.A., Go, R., Adams, J.M., 2013. pH dominates variation in tropical soil archaeal diversity and community structure. FEMS Microbiology Ecology 86, 303–311.
Vaksmaa, A., Lüke, C., Van Alen, T., Valè, G., Lupotto, E., Ettwig, K.F., 2016. Distribution and activity of the anaerobic methanotrophic community in a nitrogen-fertilized Italian paddy soil. FEMS Microbiology Ecology 92. https://doi.org/10.1093/femsec/fiw181.
Véquaud, P., Derenne, S., Anquetil, C., Collin, S., Poulenard, J., Sabatier, P., Huguet, A., 2021. Influence of environmental parameters on the distribution of bacterial lipids in soils from the French Alps: Implications for paleo-reconstructions. Organic Geochemistry 153, 104194.
Wang, H., Liu, W., Zhang, C.L., 2014. Dependence of the cyclization of branched tetraethers on soil moisture in alkaline soils from arid–subhumid China: implications for palaeorainfall reconstructions on the Chinese Loess Plateau. Biogeosciences 11, 6755–6768.
Wang, H., Liu, W., Lu, H., 2016. Appraisal of branched glycerol dialkyl glycerol tetraether-based indices for North China. Organic Geochemistry 98, 118–130.
Wang, H., Liu, Z., Zhao, H., Cao, Y., Hu, J., Lu, H., Zhao, Z., Cai, Z., Liu, X., Liu, W., 2024. New calibration of terrestrial brGDGT paleothermometer deconvolves distinct temperature responses of two isomer sets. Earth and Planetary Science Letters 626, 118497.
Weber, E.B., Lehtovirta-Morley, L.E., Prosser, J.I., Gubry-Rangin, C., 2015. Ammonia oxidation is not required for growth of Group 1.1c soil Thaumarchaeota. FEMS Microbiology Ecology 91. https://doi.org/10.1093/femsec/fiv001.
Wei, T., Simko, V., 2021. An Introduction to corrplot Package. https://cran.r-project.org/web/packages/corrplot/vignettes/corrplot-intro.html#change-color-spectra-color-legend-and-text-legend.
Weijers, J.W.H., Schouten, S., van den Donker, J.C., Hopmans, E.C., Damsté, J.S.S., 2007. Environmental controls on bacterial tetraether membrane lipid distribution in soils. Geochimica et Cosmochimica Acta 71, 703–713.
Weijers, J.W.H., Panoto, E., van Bleijswijk, J., Schouten, S., Rijpstra, W.I.C., Balk, M., Stams, A.J.M., Damsté, J.S.S., 2009. Constraints on the biological source(s) of the orphan branched tetraether membrane lipids. Geomicrobiology Journal 26, 402–414.
Wickham, H., 2009. ggplot2: Elegant Graphics for Data Analysis. Springer, New York, NY. https://doi.org/10.1007/978-0-387-98141-3.
Xiao, W., Wang, Y., Zhou, S., Hu, L., Yang, H., Xu, Y., 2016. Ubiquitous production of branched glycerol dialkyl glycerol tetraethers (brGDGTs) in global marine environments: A new source indicator for brGDGTs. Biogeosciences 13, 5883–5894.
Xie, S., Pancost, R.D., Chen, L., Evershed, R.P., Yang, H., Zhang, K., Huang, J., Xu, Y., 2012. Microbial lipid records of highly alkaline deposits and enhanced aridity associated with significant uplift of the Tibetan Plateau in the Late Miocene. Geology 40, 291–294.
Xie, W., Zhang, C., Ma, C., 2015. Temporal variation in community structure and lipid composition of Thaumarchaeota from subtropical soil: Insight into proposing a new soil pH proxy. Organic Geochemistry 83–84, 54–64.
Yang, H., Pancost, R.D., Dang, X., Zhou, X., Evershed, R.P., Xiao, G., Tang, C., Gao, L., Guo, Z., Xie, S., 2014. Correlations between microbial tetraether lipids and environmental variables in Chinese soils: Optimizing the paleo-reconstructions in semi-arid and arid regions. Geochimica et Cosmochimica Acta 126, 49–69.
Yang, H., Pancost, R.D., Jia, C., Xie, S., 2016. The Response of Archaeal Tetraether Membrane Lipids in Surface Soils to Temperature: A Potential Paleothermometer in Paleosols. Geomicrobiology Journal 33, 98–109.
Zhang, R., Wienhold, B.J., 2002. The effect of soil moisture on mineral nitrogen, soil electrical conductivity, and pH. Nutrient Cycling in Agroecosystems 63, 251–254.
Zheng, F., Chen, Y., Xie, W., Chen, S., Liu, H., Phelps, T.J., Zhang, C., 2019. Diverse biological sources of core and intact polar isoprenoid GDGTs in terrace soils from southwest of China: Implications for their use as environmental proxies. Chemical Geology 522, 108–120.